ChemComm

COMMUNICATION

View Article Online
View Journal

Cite this: DOI: 10.1039/d1cc01106e

Received 28th February 2021,
Accepted 15th April 2021

DOI: 10.1039/d1cc01106e

rsc.li/chemcomm

Co-catalytic Fc/HGQs/Fe_3O_4 nanocomposite mediated enzyme-free electrochemical biosensor for ultrasensitive detection of MicroRNA†

Liang Zhu, Xiaolong Zhang, Yuanyuan Chang, Sai Xu, Ruo Yuan and Yaqin Chai*

Herein, a novel co-catalytic ferrocene/hemin/G-quadruplexes/Fe_3O_4 nanoparticles (Fc/HGQs/Fe_3O_4) nanocomposite was synthesized to significantly magnify the electrochemical signal of ferrocene (Fc) using the synergistic catalysis of hemin/G-quadruplexes (HGQs) and Fe_3O_4 nanoparticles as hydrogen peroxide enzyme mimics for the construction of ultrasensitive electrochemical biosensors. The fabricated electrochemical biosensor can achieve ultrasensitive detection of miRNA-155 ranging from 0.1 fM to 1 nM, as well as a limit of detection of 74.8 aM. This strategy provides a new route to exploring efficient signal labels for signal amplification and provides an impetus to find novel methods for the construction of biosensors for biological detection and the early clinic diagnosis of diseases.

MicroRNAs (miRNAs) are considered to be a sort of small (roughly 19–23 nucleotides), single-stranded and non-protein-coding RNA that are expressed endogenously. They play the significant role of a regulator during the process of biological early development, cellular differentiation, proliferation, apoptosis and developmental timing, and so on.[1–4] Hence, the accurate detection of miRNAs is particularly important for early cancer diagnosis. Electrochemistry has been extensively applied to construct biosensors for precise miRNA detection, and this may be ascribed to the advantages such as a high reliability and good reproducibility.[5–7] However, most of the traditional electrochemical biosensors used simple electroactive small molecules which only act as an indicator and do not enable any amplification, and therefore the sensitivity is further restricted.[8,9] Therefore, it is necessary to explore self-enhanced electrochemical signal labels that possess stronger electrochemical signals to improve the detection sensitivity for electrochemistry analysis.

Key Laboratory of Luminescence Analysis and Molecular Sensing (Southwest University), Ministry of Education, College of Chemistry and Chemical Engineering, Southwest University, Chongqing 400715, P. R. China.
E-mail: yqchai@swu.edu.cn; Fax: +86-23-68253172; Tel: +86-23-68252277

† Electronic supplementary information (ESI) available: Experimental details, optimization of reaction conditions, feasibility of this electrochemical biosensor, selectivity, stability, and reproducibility of the prepared biosensor. See DOI: 10.1039/d1cc01106e

Herein, to overcome these issues, a synergistically catalytic material, ferrocene/hemin/G-quadruplexes/Fe_3O_4 nanoparticles (Fc/HGQs/Fe_3O_4) nanocomposite, containing hemin/G-quadruplexes (HGQs) tagged ferrocene (Fc) and Fe_3O_4 nanoparticles was synthesized as a novel co-catalytic signal label, in which the electrochemical signal response of Fc could be dramatically improved using the synergistic catalytic ability of the HGQs and Fe_3O_4 nanoparticles in the presence of H_2O_2. Compared with the conventional single signal label ferrocene (Fc) or methylene blue (MB),[10,11] the developed self-enhanced signal label Fc/HGQs/Fe_3O_4 nanocomposite possessed a much more obvious electrochemical signal response. As a proof of concept, combining the signal label Fc/HGQs/Fe_3O_4 nanocomposite with enzyme-free signal amplification, the electrochemical biosensor for the ultrasensitive detection of target miRNA-155 was successfully realized. The corresponding process and mechanism are shown in Scheme 1. Firstly, the DNA duplex Q1–H2 was attached to the interface of the gold deposited glassy carbon electrode (depAu/GCE) through Au–N bonds. With the target miRNA-155 presented, the assistant strand H1 could open, exposing the locked area and further displacing the H2 in duplex Q1–H2 (Scheme 1, step a). In this way, the miRNA-155 can be recycled by the release of duplex H1–H2 (steps c and d). Subsequently, as depicted in steps b and e, the remaining single strand Q1 on the depAu/GCE could form G-quadruplexes under the assistance of K^+ and capture amounts of the prepared signal label Fc/HGQs/Fe_3O_4 nanocomposite through π–π stacking in the presence of Mg^{2+},[12–14] thus producing an obviously multiply-amplified electrochemical signal and achieving the ultrasensitive detection of miRNA-155 with a limit of detection as low as 74.8 aM. Impressively, the developed electrochemical biosensing strategy may be used to detect the miRNA from cancer cell lysates, which provides novel insights into exploring an efficient method for the construction of a sensitive biosensor and gives an impetus to designing novel materials with significant potential for use in biosensor construction and disease diagnosis.

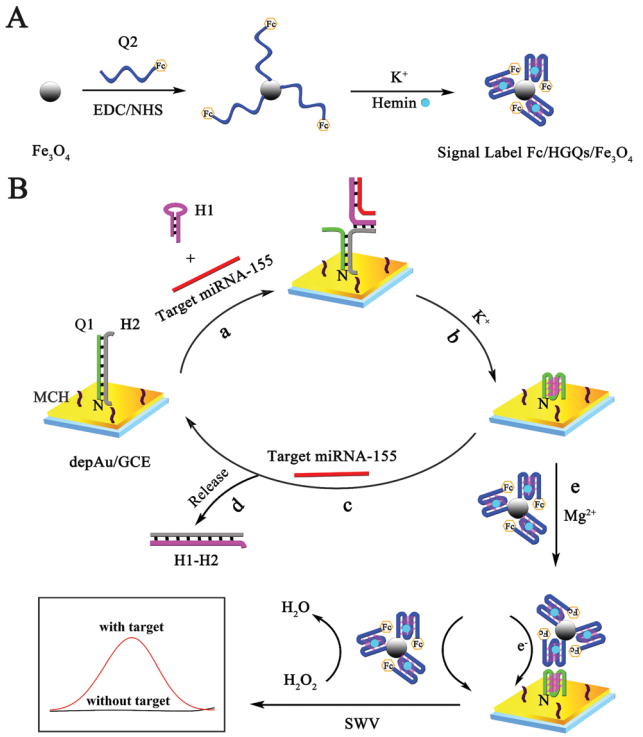

Scheme 1 Schematic representation of the fabricated electrochemical biosensor: (A) the preparation process for the signal label Fc/HGQs/Fe_3O_4 nanocomposite; (B) the mechanism of electrochemical biosensor for miRNA detection.

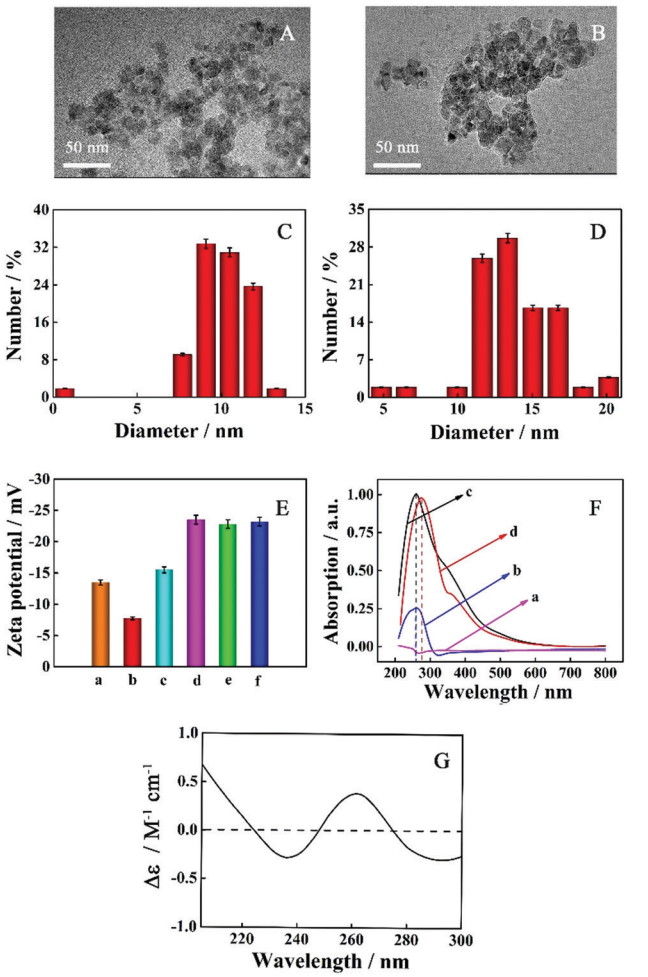

Fig. 1 TEM images of (A) the Fe_3O_4 NPs and (B) the co-catalytic Fc/HGQs/Fe_3O_4 nanocomposite. The size distribution of (C) the Fe_3O_4 NPs and (D) the Fc/HGQs/Fe_3O_4 nanocomposite. (E) Zeta potential of the: (a) Fe_3O_4 NPs, (b) Q2; (c) Fe_3O_4–Q2 reacted for 3 h; (d) Fe_3O_4–Q2 reacted for 5 h; (e) Fe_3O_4–Q2 reacted for 8 h; and (f) Fe_3O_4–Q2 reacted for 10 h, respectively. (F) UV-Vis absorption spectra of the (a) Fe_3O_4 NPs; (b) Q2; (c) Fe_3O_4–Q2; and (d) Fc/HGQs/Fe_3O_4. (G) CD spectra of 1 μM G-quadruplexes conformation formed by Q2.

Transmission electron microscopy (TEM) was carried out to characterize the morphology and size of the Fe_3O_4 nanoparticles (Fe_3O_4 NPs) and the co-catalytic signal label Fc/HGQs/Fe_3O_4 nanocomposite. As exhibited in Fig. 1A and B, the diameter of the synthesized signal label was about 13 nm, which was larger than that of the Fe_3O_4 NPs of approximately 10 nm, proving the successful synthesis of the Fc/HGQs/Fe_3O_4 nanocomposite. In addition, we carried out zeta potential measurements to certify that Q2 was immobilized onto the interface of the Fe_3O_4 NPs. Fig. 1C showed that the zeta potential of the Fe_3O_4 NPs was −13.5 mV because of the modification of the electronegative carboxyl on the interface and the potential of Q2 was −7.75 mV as a result of its own electronegativity.[15] The zeta potential of Fe_3O_4-Q2 was −15.5 mV, proving that Fe_3O_4-Q2 was synthesized successfully. Moreover, the synthesis process of the co-catalytic signal label Fc/HGQs/Fe_3O_4 nanocomposite was also characterized using ultraviolet-visible (UV-vis) spectroscopy, as depicted in Fig. 1D, there was almost no absorption of the Fe_3O_4 NPs (curve a)[16] and the absorption position of Q2 was at around 260 nm (curve b).[17] After the Fe_3O_4 NPs were modified with Q2 (Fe_3O_4–Q2), a characteristic peak appeared close to 260 nm (curve c). Furthermore, although hemin was further introduced to form Fc/HGQs/Fe_3O_4, the absorption position shifted to 282 nm (curve d) owing to the conjugative effect of the HGQs. In addition, we implemented circular dichroism (CD) to characterize the structure of the G-quadruplexes formed by Q2 in the presence of K^+. As exhibited in Fig. 1E, the CD spectra with a negative peak at 238 nm and a positive peak at 260 nm is usually interpreted as the formation of the G-quadruplexes conformation, which is consistent with the results of previous studies.[18] These characterization results illustrated that the Fc/HGQs/Fe_3O_4 nanocomposite was successfully synthesized.

The electrochemical characterizations of the stepwise-modified electrode were accomplished through cyclic voltammetry (CV) and electrochemical impedance spectroscopy (EIS). As displayed in Fig. 2A, firstly, a characteristic redox peak of $[Fe(CN)_6]^{3-/4-}$ was acquired using the bare electrode (curve a). Subsequently, the current increased remarkably (curve b) once the gold particles (depAu) were modified onto the electrode on account of the pre-eminent conductivity of depAu. After the DNA strands were attached to the electrode surface, an obviously decreased peak current appeared owing to the repulsive interaction between the electronegative phosphate backbone of the DNA and $[Fe(CN)_6]^{3-/4-}$ (curve c). Next, a dramatically decreased peak

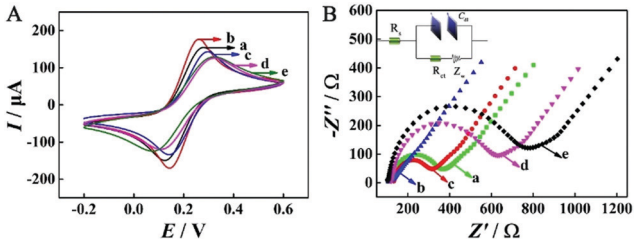

Fig. 2 (A) CV and (B) EIS of the (a) bare GCE; (b) depAu/GCE; (c) Q1–H2/depAu/GCE; (d) MCH/Q1–H2/depAu/GCE; and (e) H1-miRNA-155/MCH/Q1–H2/depAu/GCE.

current was observed after 6-mercapto-1-hexanol (MCH) was added to occupy the nonspecific binding sites (curve d). Then, the mixture of hairpin DNA H1 and miRNA-155 was fixed on the electrode, and a slightly decreased current response value (curve e) was acquired owing to the steric hindrance of the G-quadruplexes.

The EIS of the modified electrode is shown in Fig. 2B. In comparison with the bare GCE (curve a), a significantly decreased electron transfer resistance (R_{et}) value was obtained for depAu/GCE (curve b) owing to the good conductivity of depAu. After adding duplex DNA Q1–H2 to the electrode surface, the R_{et} of the modified electrode increased obviously owing to the increased steric hindrance as a result of the modification of Q1–H2 (curve c). Subsequently, when the MCH and the mixture of miRNA-155 and H1 were modified on the above mentioned electrode in a stepwise manner, a series of successive increases of the R_{et} could be observed owing to the incremental steric hindrance on the surface of the electrode (curves d and e). The findings were in agreement with the phenomenon observed using CV, indicating that this biosensor was successfully constructed.

To prove that the co-catalytic signal label Fc/HGQs/Fe_3O_4 nanocomposite significantly enhanced the electrochemical signal response, a comparison of the signal response of the different biosensors was then performed. As depicted in Fig. 3, in the presence of H_2O_2, a low electrochemical signal response for the biosensor was obtained with a G-quadruplexes conformation of Q2 acting as a signal label (curve a). Nevertheless, the corresponding signal response of the biosensor with HGQs or Fe_3O_4-G-quadruplexes acting as a signal label was around three times greater than that of the G-quadruplexes acting as a signal label (curves b and c, respectively), verifying that all the HGQs or Fe_3O_4 could enhance the electrochemical signal of Fc. Impressively, although hemin and Fe_3O_4 were simultaneously introduced to form Fc/HGQs/Fe_3O_4 as a signal label, the signal response value dramatically increased to 18.7 μA (curve d), which was almost nine times that obtaining using the G-quadruplexes as a signal label. The results showed that synergistic catalysis of the HGQs and Fe_3O_4 in Fc/HGQs/Fe_3O_4 could indeed significantly improve the signal response and further enhance the sensitivity for examining miRNA.

The biosensor was incubated with a series of concentrations of miRNA-155 and monitored *via* square wave voltammetry (SWV) using the optimum experimental conditions, respectively. As depicted in Fig. 4A, the electrochemical signal responses

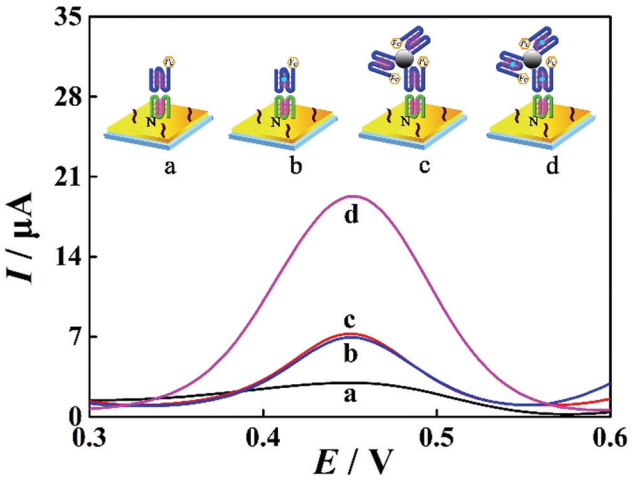

Fig. 3 The SWV responses of different biosensors with 1 nM miRNA-155 and the following signal label: (a) G-quadruplexes; (b) HGQs; (c) Fe_3O_4-G-quadruplexes; and (d) Fc/HGQs/Fe_3O_4, respectively. Detection buffer: 2 mL of PBS (pH = 7.4) containing H_2O_2 (1.38 mmol L^{-1}). Illustration above shows the different signal labels on the surfaces of the electrode corresponding to a–d, respectively.

enhanced gradually as miRNA-155 ranged from 0.1 fM to 1 nM and displayed an excellent linearity with the logarithm of the concentrations of miRNA-155. The calibration plot is shown in Fig. 4B and the corresponding linear regression equation is $I = 41.40 + 2.557 \lg c_{\text{miRNA-155}}$ ($r = 0.9905$), which shows a limit of detection of 74.8 aM (LOD = $3S_B/m$). As depicted in Table S2 (ESI†), compared with the previous studies, the proposed biosensor possessed a greater sensitivity for detecting miRNA-155 and possessed a wide response range. In addition, as illustrated in Fig. S3 (ESI†), this fabricated biosensor displayed excellent selectivity, stability, and reproducibility.

The biosensor could be used to detect lysates from human breast cancer cells (MCF-7) and cervical cancer cell lines (HeLa). As illustrated in Fig. 5, an obvious signal response enhancement was observed when the numbers of MCF-7 and HeLa increased from 10^2 to 10^4, indicating the overexpression of miRNA-155 in the MCF-7 and HeLa, which was in accordance with the results reported in previously published reports.[19,20] Therefore, all of the obtained results proved that the prepared

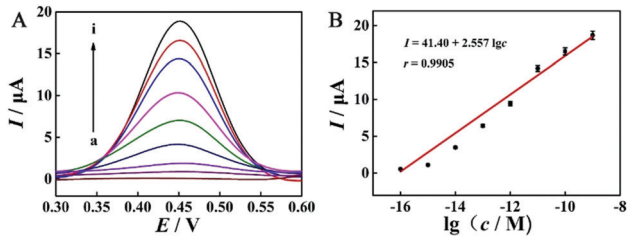

Fig. 4 (A) SWV response of the fabricated biosensor under different miRNA-155 concentrations: (a) 0 fM; (b) 0.1 fM; (c) 1 fM; (d) 10 fM; (e) 100 fM; (f) 1 pM; (g) 10 pM; (h) 100 pM; and (i) 1 nM. (B) The calibration plot of *I versus* the logarithm of miRNA-155 concentration. Error bars, SD; $n = 3$.

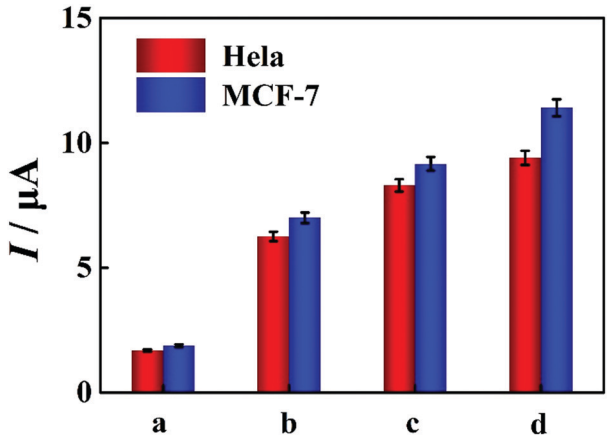

Fig. 5 Detection of miRNA-155 from extracts of MCF-7 and HeLa: (a) blank (without target miRNA-155), (b) 10^2 cells, (c) 10^3 cells, and (d) 10^4 cells.

biosensor possessed the potential to detect miRNA-155 in practical samples.

In this work, by combining the co-catalytic signal label Fc/HGQs/Fe_3O_4 nanocomposite as an electrochemical signal label with enzyme-free target recycling amplification (EFTRA) as a signal amplifier, an electrochemical biosensor was constructed for ultrasensitive detection of miRNA-155. There are two advantages of this proposed biosensor: first, the catalytic action of the Fe_3O_4 nanoparticles (Fe_3O_4 NPs) and hemin/G-quadruplexes (HGQs) on H_2O_2 accelerated the transfer of electrons in the system, resulting in an obvious increase in the electrochemical signals; second, the enzyme-free target recycling amplification process also contributed to the amplification of the electrochemical signal response to further increase the electrochemical biosensor sensitivity. This method could be applied for the analysis of many other biomarkers and for enhancing efficiency in early clinic diagnosis.

Liang Zhu: conceptualization, data curation, formal analysis, investigation, writing – original draft, writing – review & editing. Xiaolong Zhang: conceptualization, writing – original draft, supervision. Yuanyuan Chang: funding acquisition. Sai Xu: conceptualization, writing – original draft, supervision. Ruo Yuan: funding acquisition, resources, project administration, supervision. Yaqin Chai: funding acquisition, resources, Writing – review & editing.

This paper was financially supported by the National Natural Science Foundation of China (21775124, 21974108 and 21675129), the Fundamental Research Funds for the Central Universities (XDJK2019TJ002), China Postdoctoral Science Foundation (2019M663417 and 2020T130544) and the Postdoctoral Science Foundation of Chongqing Natural Science Foundation (cstc2020jcyj-bsh0026).

Conflicts of interest

There are no conflicts to declare.

Notes and references

1 L. M. Xian, F. Xu, J. Z. Liu, N. Xu, H. D. Li, H. Y. Ge, K. Shao, J. L. Fan, G. S. Xiao and X. J. Peng, *J. Am. Chem. Soc.*, 2019, **141**, 20490–20497.
2 L. J. Wang, M. Ren, H. X. Wang, J. G. Qiu, B. H. Jiang and C. Y. Zhang, *Anal. Chem.*, 2020, **92**, 8546–8552.
3 S. Zhang, S. Xu, R. Ma, G. Cheng, Q. Xue and H. Wang, *Chem. Commun.*, 2020, **56**, 4288–4291.
4 M. T. Gabr and F. Barbaultb, *Chem. Commun.*, 2020, **56**, 9695–9698.
5 Y. R. Li, Y. Y. Chang, J. Ma, Z. Y. Wu, R. Yuan and Y. Q. Chai, *Anal. Chem.*, 2019, **91**, 6127–6133.
6 A. Bagheri Hashkavayi, B. S. Cha, E. S. Lee, S. Kim and K. S. Park, *Anal. Chem.*, 2020, **92**, 12733–12740.
7 W. He, B. Qiao, F. Z. Li, L. S. Pan, D. L. Chen, Y. Cao, J. C. Tu, X. H. Wang, C. Z. Lv and Q. Wu, *Chem. Commun.*, 2021, **57**, 619–622.
8 J. Jiang, H. Y. Wu, Y. Su, Y. Liang, B. W. Shu and C. S. Zhang, *Anal. Chem.*, 2020, **92**, 7708–7716.
9 X. L. Zhang, Z. H. Yang, Y. Y. Chang, D. Liu, Y. R. Li, Y. Q. Chai, Y. Zhuo and R. Yuan, *Chem. Sci.*, 2020, **11**, 148–153.
10 Y. Dai, R. A. Somoza, L. Wang, J. F. Welter, Y. Li, A. I. Caplan and C. C. Liu, *Angew. Chem., Int. Ed.*, 2019, **58**, 17399–17405.
11 Q. Hu, Y. Bao, S. Y. Gan, Y. W. Zhang, D. X. Han and L. Niu, *Anal. Chem.*, 2020, **92**, 3470–3476.
12 N. Smargiasso, F. Rosu, W. Hsia, P. Colson, E. S. Baker, M. T. Bowers, E. D. Pauw and V. Gabelica, *J. Am. Chem. Soc.*, 2008, **130**, 10208–10216.
13 W. Ren, Y. Zhang, H. G. Chen, Z. F. Gao, N. B. Li and H. Q. Luo, *Anal. Chem.*, 2016, **88**, 1385–90.
14 C. Ye, M. Q. Wang, H. Q. Luo and N. B. Li, *Anal. Chem.*, 2017, **89**, 11697–11702.
15 Y. He, X. Li, Z. Li, J. Bian, X. Zhang, S. Wei, X. Zhang and D. Gao, *Chem. Commun.*, 2020, **56**, 10533–10536.
16 A. Dutta Chowdhury, N. Agnihotri, R.-A. Doong and A. De, *Anal. Chem.*, 2017, **89**, 12244–12251.
17 S. Kundu and H. Liang, *Adv. Mater.*, 2008, **20**, 826–831.
18 C. Ghimire, S. Park, K. Iida, P. Yangyuoru, H. Otomo, Z. Yu, K. Nagasawa, H. Sugiyama and H. Mao, *J. Am. Chem. Soc.*, 2014, **136**, 15537–44.
19 S. Z. Yue, X. Y. Song, W. L. Song and S. Bi, *Chem. Sci.*, 2019, **10**, 1651–1658.
20 Z. Z. Yang, X. Peng, P. Yang, Y. Zhuo, Y. Q. Chai, W. B. Liang and R. Yuan, *Chem. Sci.*, 2020, **11**, 8482–8488.

